RANDOM VORTEX METHOD FOR THREE DIMENSIONAL FLOWS. PART II: NUMERICAL IMPLEMENTATION AND SAMPLE RESULTS [1]

Andrzej Styczek
Piotr Duszyński
Marta Poćwierz
Jacek Szumbarski

Institute of Aeronautics and Applied Mechanics, Warsaw University of Technology
e-mail: jasz@meil.pw.edu.pl

Continuation of the first part of the paper focuses on implementation issues, computational efficiency and presentation of test calculations. Sample results have been obtained for a viscous flow past a spherical body immersed in an uniform stream. The solution algorithm for the external Neumann boundary problem, the construction of the vortex particles near the material boundary and the evaluation of the stretching effect are described in some details. The problem of design of efficient algorithms for induced velocity computation is discussed briefly. The presented results include patterns of instantaneous velocity and vorticity field as well as selected streamlines showing the complexity of flow near the aft part of the body and inside the aerodynamic wake.

Key words: vortex methods, vortex stretching, Fokker-Planck-Kolmogorow equation, Itô stochastic differential equations

1. Introduction

In the first part of the paper Styczek *et al.* (2004), the Lagrangian vortex method for 3D viscous flows has been formulated. Here, certain implementation issues are discussed and sample results are presented. The focus is on the investigation of the algorithm features rather that on solving a particular

---

[1]*Part I: Mathematical background* has been published in Journal of Theoretical and Applied Mechanics, **42**, 1, 2004

physical problem. Our test case is the flow past a spherical body, which is geometrically simple but still nontrivial due to appearance of complex vortex patterns of the wake behind the body. Simple geometry of the flow domain facilitates an efficient numerical solution to the external Neumman boundary problem for the Laplace equation, which is conceptually the most complex element of the proposed method. An other essential element – solving the Ito stochastic differential equations for vortex trajectories of the particles – is not a difficult task. Since the diffusion coefficient is constant, these equations are in fact of the Stratonowicz type, and as such can be integrated using standard numerical procedures (see Gardiner, 1990). The crucial problem is a computational rather that theoretical one: how to calculate quickly the induced part of the velocity field.

The sample results presented in this work include patterns of instantaneous velocity and vorticity fields, instantaneous streamlines and vortex spatial distribution of the particles. The Reynolds number assumed in the numerical simulations is the range where the wake behind the sphere becomes essentially unstable, loses symmetry and the small-scale motion inside it develops complicated, apparently chaotic behavior.

The obtained results show good and weak points of the proposed method. The sources of difficulties and measures to avoid them are discussed in some extent.

2. The numerical method for the external Neumann boundary problem

In order to calculate auxiliary potentials φ_U, φ_O and φ_{ki}, needed for the velocity determination (Eqs (4.7), (6.5), (6.6) and (6.8) of the Part I), the external Neumann boundary value problem for the Laplace equation has to be solved.

The boundary condition for each of these problems can be written in the following form

$$\frac{\partial \varphi}{\partial n} = \frac{\partial \varphi}{\partial r}\Big|_{r=R} = f(\theta, \gamma) \tag{2.1}$$

In the above, φ denotes a harmonic function in the exterior domain $|\boldsymbol{r}| \equiv r > R$, and the function f is given and depends on the particular case considered. All boundary problems are well posed, meaning that

$$\oint f(\theta, \gamma) \cos \theta \, d\theta d\gamma = 0 \tag{2.2}$$

The symbols θ and γ denote the spherical coordinates on the sphere: the longitudinal and azimuthal angles, respectively.

The solution can be expressed in the well-known form of the infinite series

$$\varphi = -R \sum_{n=1}^{\infty} \frac{Y_n(\theta, \gamma)}{n+1} \left(\frac{R}{r}\right)^{n+1} \tag{2.3}$$

In the above, $Y_n(\theta, \gamma)$ is a spherical function of the nth order. With the use of boundary conditions (2.1), one gets

$$f(\theta, \gamma) = \sum_{n=1}^{\infty} Y_n(\theta, \gamma) = \sum_{n=1}^{\infty} \sum_{m=0}^{n+1} C_n^m P_n^m(\cos\theta) e^{in\gamma} \tag{2.4}$$

The symbol P_n^m denotes associated Legendre polynomials, i.e.

$$P_n^m(x) = (1 - x^2)^{\frac{m}{2}} \frac{d^m P_n(x)}{dx^m}$$

where the Legendre polynomials $P_n(x)$ are defined as

$$P_n(x) = \frac{1}{n! 2^n} \frac{d^n}{dx^n} (x^2 - 1)^n$$

The expansion coefficients C_n^m can be found by means of the standard harmonic analysis on the sphere (Chorlton, 1969).

3. Computing the trajectories of the vortex particles

As described in Part I (see Section 5, Eq. (5.5)), the trajectory of the center of a vortex particle is described by the stochastic differential equation

$$d\boldsymbol{r}_i = \boldsymbol{v}_i dt + \sqrt{2\nu}\, d\boldsymbol{W}_i \tag{3.1}$$

The increment of the Wiener process $d\boldsymbol{W}_i$ can be defined as

$$d\boldsymbol{W}_i = \sqrt{dt}\, \boldsymbol{\xi}_i$$

where $\boldsymbol{\xi}_i$ is the random vector whose components are statistically independent variables with the standard Gaussian distribution $N(0,1)$.

The velocity at the particle center $\boldsymbol{v}_i$ is computed by summing up the induction and other components accordingly to formula (4.7) from Part I.

We also already mentioned that stochastic differential equations (3.1) can be integrated using standard numerical methods (the viscosity of a fluid is constant). The trajectories of the vortex particles are traced using the multi-step integration scheme of the 3rd order, except for newly created particles, whose trajectories are initially calculated using a low-order single-step scheme. The important problem is the choice of initial conditions, i.e. the initial locations of the newly created particles. When these points are projected orthogonally onto the sphere, a surface grid is obtained. Putting things the opposite way, each surface grid on the sphere can be used to generate a set of initial positions for the vortex particles. It seems, however, that some types of the grid (like the geographical one or the grid based of the polyhedral division) may not be appropriate, because they would introduce particular symmetries, which might lead to artifacts in the vorticity and velocity fields. Therefore, a grid generation algorithm based on the maximization of the following measure

$$D = \sum_{i,j} |\boldsymbol{r}_i^{srf} - \boldsymbol{r}_j^{srf}| \qquad (3.2)$$

has been implemented. In the above, $\boldsymbol{r}_i^{srf} - \boldsymbol{r}_j^{srf}$ is the vector linking ith and jth points of the surface grid on the sphere.

The set of surface points maximizing the measure D can be determined iteratively. In each iteration, the surface points are moved along the vectors

$$\boldsymbol{w}_i = \sum_j \frac{\boldsymbol{r}_i - \boldsymbol{r}_j}{|\boldsymbol{r}_i - \boldsymbol{r}_j|} \varepsilon$$

(ε denotes a small parameter introduced in order to restrict the magnitude of the displacements of the surface points), and then projected orthogonally back onto the sphere. Note that the vectors $\boldsymbol{w}_i$ are parallel to the gradient of the measure D, hence the described procedure leads to magnification of this measure. Numerical computations show that the mesh generation algorithm works correctly and efficiently. The iterations are terminated until the modification of D becomes negligible. Since the obtained locations are not changed during flow simulation, the numerical cost of the above algorithm is not relevant.

Having the grid points on the spherical surface, one can consider the set of lines emanating from these points and pointing outside in the normal directions. New vortex particles are initially located on these lines and the distance from the surface is such that the tangent component of the induced velocity is maximal. Note that the radius of the particle σ (see formula (3.8) from Part I) and the optimal distance are connected accordingly to the form of the core function $f(r)$.

4.   Computation of the stretching effect

The effect of the vortex stretching is described by Eq. (5.7) given in Styczek *et al.* (2004)

$$\partial_t \boldsymbol{\omega} = (\boldsymbol{\omega} \cdot \nabla)\boldsymbol{v} \equiv \frac{d}{d\lambda} \boldsymbol{v}(t, \boldsymbol{r} + \lambda \boldsymbol{\omega})\Big|_{\lambda=0}$$

Using the representation of the vorticity field for a single vortex particle we obtain (see Section 6 of Part I)

$$\frac{d\boldsymbol{\Omega}_k}{dt} = \frac{3}{2f(0)} \frac{d}{d\lambda} \boldsymbol{v}(t, \boldsymbol{r} + \lambda \boldsymbol{\omega}(t, \boldsymbol{r}_k))\Big|_{\lambda=0} \tag{4.1}$$

The same result can be derived the other way. Indeed, integration of the stretching equation within a ball with the radius r_0, followed by calculations similar to those in Section 3 in Styczek *et al.* (2004), yields

$$\int \partial_t \boldsymbol{\omega}_k(t, \boldsymbol{\xi}) \, d_3\boldsymbol{r} = 4\pi \boldsymbol{\Omega}'_k(t) \left[\int_0^{r_0} \xi^2 f(\xi) \, d\xi - \int_0^{r_0} \frac{F(\xi)}{\xi} \, d\xi \right] -$$

$$-\frac{4\pi}{3} \boldsymbol{\Omega}'_k \left[\int_0^{r_0} \xi^2 f(\xi) \, d\xi - 3 \int_0^{r_0} \frac{F(\xi)}{\xi} \, d\xi \right] = \int_{S(r_0)} (\boldsymbol{n}\boldsymbol{\omega})\boldsymbol{v}(t, \boldsymbol{r}) \, dS(r_0)$$

Using the following relation between the functions $f(r)$ and $F(r)$

$$F(r) = \int_0^r \xi^2 f(\xi) \, d\xi$$

some terms in the above expression cancel out, and finally we get

$$\boldsymbol{\Omega}'_k(t) = \frac{\int_{S(r_0)} (\boldsymbol{n}\boldsymbol{\omega})\boldsymbol{v}(t, \boldsymbol{r}) \, dS(r_0)}{\frac{8\pi}{3} \int_0^{r_0} \xi^2 f(\xi) \, d\xi} \tag{4.2}$$

Assuming r_0 very small, the following approximation is admissible

$$\boldsymbol{\Omega}'_k(t) \approx \frac{(\boldsymbol{\omega}\nabla)\boldsymbol{v}}{\frac{2}{r_0^3} \int_0^{r_0} \xi^2 f(\xi) \, d\xi} = \frac{(\boldsymbol{\omega}\nabla)\boldsymbol{v}}{\frac{2}{3} f(0)}$$

The velocity vector $\boldsymbol{v}$ contains the contribution induced by the kth particle. We will derive closed formulae describing the part of the vortex stretching

due to the interaction between the jth and kth particles. The sum of these contributions over the indices $i = 1, 2, 3, \ldots$ defines the total stretching effect of the vorticity-induced component of the velocity field on the kth particle. The remaining part of the stretching is due to the potential component and can be computed by numerical differentiation in the direction of the vorticity vector in the particle centre. In order to derive necessary formulas, we use a local coordinate system with the origin at the particle centre. Next, we have

$$
\begin{aligned}
\boldsymbol{s}(\boldsymbol{r}, j, k) &= \frac{d}{d\lambda} \frac{\boldsymbol{\Omega}_j \times (\boldsymbol{r} + \lambda \boldsymbol{\Omega}_k)}{|\boldsymbol{r} + \lambda \boldsymbol{\Omega}_k|^3} F(|\boldsymbol{r} + \lambda \boldsymbol{\Omega}_k|)\Big|_{\lambda=0} = \\[2mm]
&= \left[\frac{\boldsymbol{\Omega}_j \times \boldsymbol{\Omega}_k}{r^3} - \frac{3(\boldsymbol{\Omega}_k \boldsymbol{r})(\boldsymbol{\Omega}_j \times \boldsymbol{r})}{r^5} \right] F(r) + \frac{(\boldsymbol{\Omega}_k \boldsymbol{r})(\boldsymbol{\Omega}_j \times \boldsymbol{r})}{r^2} f(r)
\end{aligned}
\tag{4.3}
$$

The problem arises when the interacting particles have their centers in the same point. If $r \to 0$, the second and the third terms in (4.3) cancel each other since

$$
\lim_{r \to 0} \frac{F(r)}{r^3} = \lim_{r \to 0} \frac{1}{r^3} \int_0^r \xi^2 f(\xi)\, d\xi = \frac{1}{3} f(0)
$$

The first term in (4.3) will vanish if only $f(0) = 0$. The reason for such an assumption is the avoidance of the pathological self-stretching effect.

Summing up all contributions defined by (4.3), we get

$$
\boldsymbol{S}(k) = \sum_j \boldsymbol{s}(\boldsymbol{r}_k - \boldsymbol{r}_j, j, k)
\tag{4.4}
$$

which determines the vorticity-induced part of the derivative $\boldsymbol{\Omega}_k'(t)$. The stretching effect due to the potential part is calculated numerically using the central finite difference formula of the second order in the direction of the unary vector $\boldsymbol{\Omega}_k / \Omega_k$.

5. Computation of the vortex interaction (induced velocity)

Usability of the method of vortex particles in 3D is mostly determined by its computational efficiency. Like in any particle method, the numerical cost of induced velocity evaluation is proportional to the squared number of the vortex particles. The stretching determination is also expensive since it requires additional calculation of the velocity field at two points near each particle center. Another time-consuming part of the algorithm is the determination

of the right-hand side vector of the linear system for the charges of the new particles. Although its cost increases only linearly with the number of particles, there is a large computational "overhead" due to complicated expressions involved. Other elements of the algorithm give rather negligible contributions to the overall CPU effort.

The most crucial for computational effectiveness is the reduction of time for the induced velocity evaluation. It seems that the simplest idea is to introduce an interpolation grid. The mutual induction of close particles is computed from exact formulas on each-to-each basis. The induction of distant particles is calculated indirectly: first the velocity at the grid vertices is determined and next it is interpolated from the vertices to the particle centers. The major drawback of such approach is that simple interpolation rules cannot be divergent free and vice versa. Besides, this method works efficiently only if the spatial distribution of the particles is sufficiently uniform, which is rarely a case, especially for wake flows behind immersed bodies.

Other, much more sophisticated approaches to interacting particles have been proposed since late '80s. The most popular ones are:

- methods based on the usage of multipole expansions, the most eminent example being the famous Greengard-Rokhlin's Fast Multipole Method (FMM) (see Pringle (1994) for comprehensive survey of this approach),

- methods using tree structures, for example the Bernes-Hut algorithm (see Blelloch and Narlikar, 1997).

Both algorithms have their pros and cons. The BH algorithm is easier to implement but it offers worse performance, especially when higher accuracy is demanded Blelloch and Narlikar, 1997. With a moderate number of particles (say, 50 thousands), the numerical cost related to error reduction by one order of magnitude in the BH method is nearly the same as the cost of error reduction by three orders in FMM (Gibbon, 2002). The main disadvantage of the latter is, in turn, high complexity of (recursive) implementation, which results in a large computational "overhead". In effect, the FMM can significantly accelerate computations (say of one order of magnitude), but only if the number of the vortex particles increases well over fifty thousands (Gibbon, 2002).

In the current work, the numerical simulations have been carried out with a few hundreds of the vortex particles injected into the flow domain in each time step. The number of the particles increases almost linearly and achieves several tens of thousands at the end of the simulation. With the currently available hardware, we have found it impractical to carry on with a larger number of particles. In view of the efficiency limitations of the fast summation algorithms

mentioned above, it seemed reasonable to use a direct method for the induced velocity. In order to reduce computational times, partial parallelization of the codes using MPI libraries have been attempted. The parallelization has been applied to the most time consuming part of the computations, namely:

- evaluation of the mutual induction of the vortex particles,
- calculations of the stretching effect due to the induced velocity (the part of the stretching due to potential components has been calculated sequentially),
- calculations of the right-hand sides of the linear system for newly created particles.

The parallel computations have included three stages. In the first stage, all necessary data concerning the particles have been sent over to all processors. Next, each processor performed calculation for its individual portion of the particles. Finally, all results have been sent back to the main processor.

6. Numerical test case: flow past a spherical body

The vortex method described above has been tested extensively on the example of a viscous flow past a spherical body immersed in a uniform stream with $u_\infty = 1$. The obtained results include trajectories of the particles and instantaneous patterns of the velocity and vorticity. In order to visualize the flow complexity, selected streamlines of an instantaneous velocity have also been calculated.

In all presented cases, the flow has been accelerated from rest. During the initial short time interval, the free stream velocity u_∞ was increased from zero to unity and then kept fixed. The time step $\Delta t = 0.01$ was found a reasonable compromise between the accuracy and computational efficiency. With a smaller time step, the number of the vortex particles grew much faster, making long lasting simulation not feasible because of the hardware limitations.

As it has been already described, the vortex particles are shed from the region near the body surface and then moved downstream forming the wake behind the body. A large portion of the particles drops into the area right behind the body and remains there for a rather long time. Such behavior is natural from a dynamical point of view – the area of the near wake is occupied by a large, nearly toroidal, vortex structures which take a mass of the flow from the separated boundary layer and push it towards into the wake
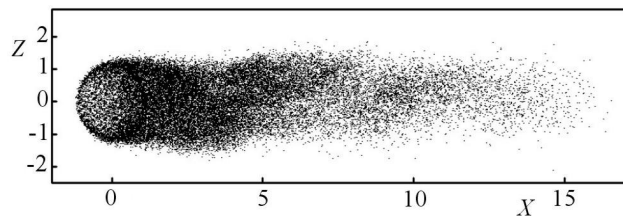
Fig. 1.

interior and into the aft part of the body. From the computational point of view, this phenomenon is an example of the characteristic feature of all vortex methods: they have natural ability to self-adapt the spatial resolution in the dynamically active regions of the flow field. Figure 1 shows instantaneous locations of the vortex particles obtained for the Reynolds number $Re = 200$ and the simulation time $t = 16$. The number of the particles generated at each time step in the vicinity of the body surface was set to 400. The number of the particles in the flow field was about 40 thousands. Darkly shaded area just behind the body shows how large portion of the particles is "trapped" in the near-wake structures. Another important feature is the asymmetric form of the wake – its wavy shape, observed also in other simulations and in experiments, is apparent.

The instantaneous patterns of the velocity field are presented for three different values of the Reynolds number. In Fig. 2, the projection of the velocity on the XZ plane is presented. The Reynolds number is equal: 100 (Fig. 2a), 200 (Fig. 2b) and 400 (Fig. 2c). In all cases, the number of the particles generated in each time step was equal to 400, and all velocity patterns corresponded to the same time instant $t = 9.2$.

The flow field obtained for $Re = 100$ is remarkably symmetric. The vortex structure in the form of a flattened toroid, extending along the wake at a distance of about one diameter of the sphere is visible. The obtained wake symmetry is in good agreement with the experimental observation for the same Reynolds number.

The comparison with the velocity fields obtained for larger Reynolds numbers reveals gradual development of the asymmetry in the wake flow. Moreover, the velocity irregular profiles of the reversed flow in the central part of the wake observed for $Re = 400$ appear due to a more complicated and containing more that one large vortex structure flow pattern. The development of the wavy shape of the wake in the streamwise direction can be inferred from the most right velocity vectors in Fig. 2c (for X coordinate between 6 and 7). The
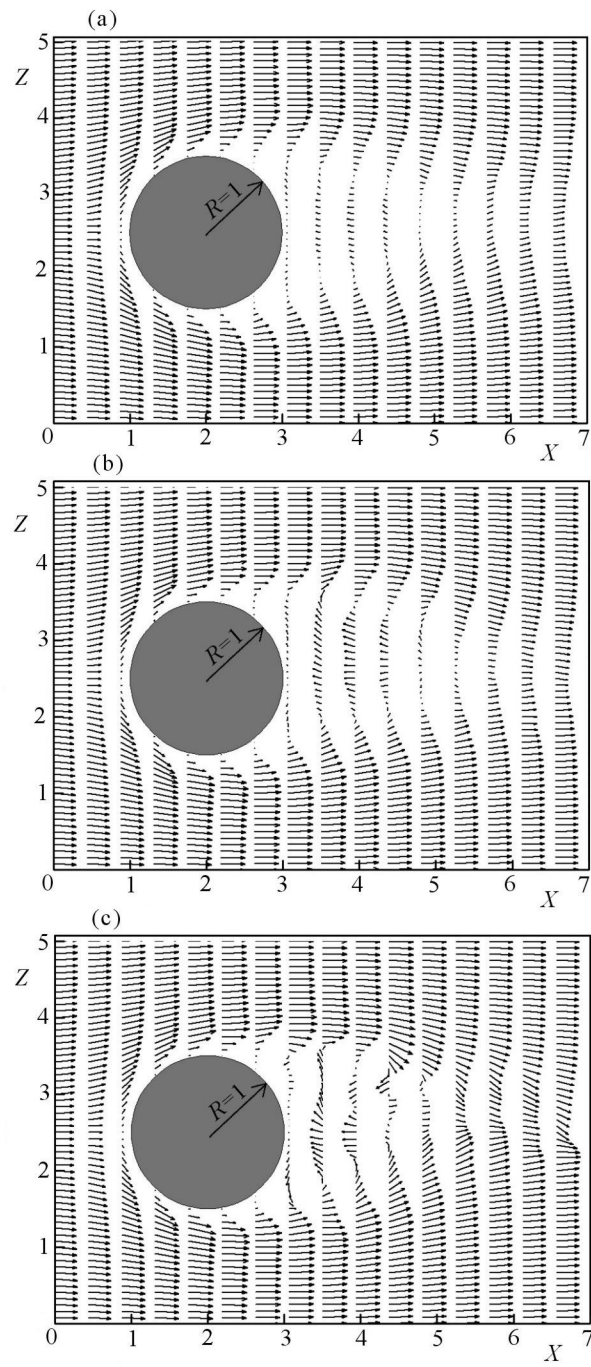
(a)

(b)

(c)

Fig. 2.

shape of the flow at Re = 200 exhibits an intermediate character: it is still very regular but the first symptoms of the symmetry breaking are already visible. The overall picture of the wake flow dynamics in the considered range of the Reynolds number seems to be qualitatively similar to the results of recent vortex simulation by Ploumhans *et al.* (2002).
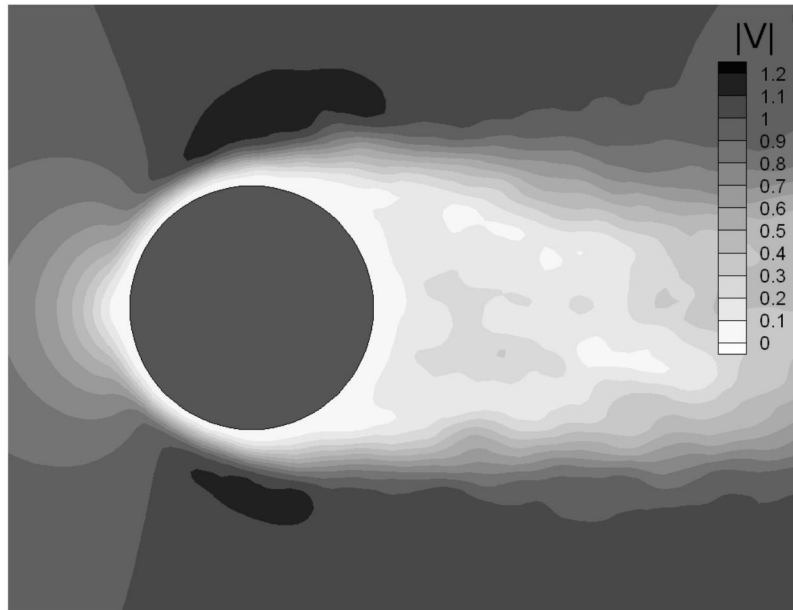

Fig. 3.

For better visualization of the flow structures, the contour maps of the magnitude of the XZ-projection of the velocity and Y-component of the instantaneous vorticity field are presented in Fig. 3 and Fig. 4, respectively. The corresponding flow has been calculated for Re = 100 and the time instant $t = 17$. The large-scale symmetry seen before on the vector maps, especially in the near wake, is now less apparent, which may be partly explained by the choice of a much later time instant. The vorticity map presents some small-scale details of the flow. It turns out that regions of largest vorticity are located near the body surface (as expected) and on the "edges" of the wake. The latter observation is rather not trivial as one might expect that the area of the large vorticity would be located closer to the center line of the wake, namely in the vicinity of points where the direction of the wake flow is altered.

In spite of the apparent global symmetry, the small-scale motion obtained in the vortex simulation can be remarkably complicated. In Fig. 5 we show two
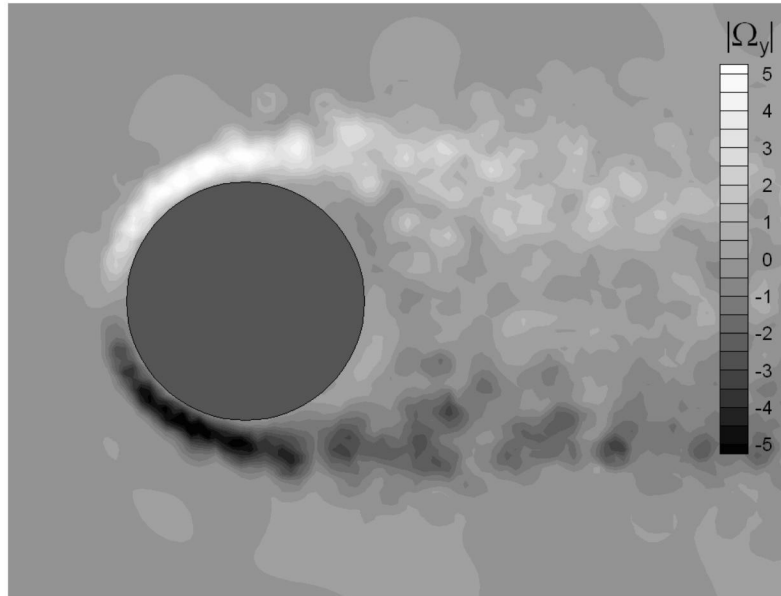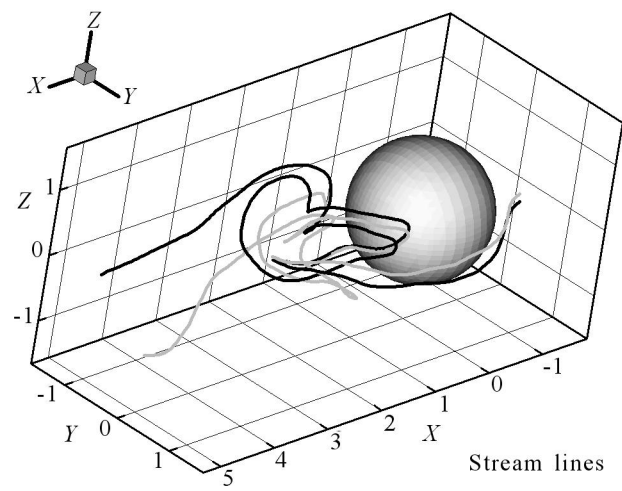
Fig. 4.

Fig. 5.

streamlines of the instantaneous velocity field calculated for $Re = 200$ at the time instant $t = 17$. The streamlines originate from two points located in the upstream direction and close to each other. As long as the streamlines go near the body surface they remain close and have a similar shape. The situation changes drastically when they enter the wake region. The dynamics in the "frozen" velocity field behind the body (here the streamlines are interpreted as trajectories of the marker particles moving in pseudo-time in the fixed velocity field) is highly sensitive to initial conditions meaning that two, initially close, trajectories diverge rapidly wiggling around the whole area in a complicated manner.

While the presented results show the capability of the proposed vortex method to model a wake flow behind a bluff body realistically, they also reveal its major weakness: poor quality of representation of thin shear layers near the material surface. It is evident from the vector maps in Fig. 2 than the velocity gradients at the surface are much smaller that in a real flow (also the general tendency, i.e. "the larger Re the larger gradients" is weakly marked). In effect, the friction drag is vastly underestimated. Also, it is difficult to say to what extent the shift of the large vorticity off the wake center is merely the artifact of the thick boundary layer and its premature separation.

The source of the above difficulty is in the particle's geometry and, partly, in hardware limitations. In a sense, each vortex particle occupies the whole space (see Part I) but it is mostly concentrated in a rather small spherically symmetric vicinity of its central point characterized by the magnitude of the "core" radius σ. Such vorticity carriers are very convenient to use because of simple analytical induction formulae. Besides, in contrast to the "vortex particles" used by some researchers, the vorticity of the particles constructed in this work is a well-defined divergent-free vector field. On the other hand, the spherical symmetry of these objects does not make them well suited for approximations of a flow field with highly anisotropic geometry in a kind of a boundary layer, unless their core radii are very small. The latter, however, brings huge computational efficiency problems. If the particles are small then the number of the vortex particles necessary to enforce the no-slip condition with a reasonable accuracy becomes very large. The reason for this is rather obvious. If the body surface was loosely covered with a small number of tiny particles then the accuracy of cancellation of the tangential velocity component (set to zero only in a small number of collocation points) would be very poor.

A possible way of overcoming the efficiency limitations and achieving a satisfactory resolution in the transversal direction of the boundary layer is to introduce some "flattened" vortex structures. The crucial question is how to

construct such particles, so that the corresponding induction formulae (probably not explicit anymore) can be computed quickly. Additionally, such an idea is a source of further arbitrariness in the method, namely, the problem arises when and how a "flat" vortex particle is to be replaced by an "ordinary" (spherical) one.

A radical approach is to resign from the particle approximation of the flow in the closest vicinity of the body and use the concept of a singular vorticity layer. The no-slip boundary condition is realized by a surface distribution of discontinuity of the tangent velocity component determined as a solution to the appropriate boundary integral equation. The magnitude of a local discontinuity determines the equivalent local flux of the vorticity through the body surface. The vorticity production (or destruction) is realized by injection (or removal) of the adjacent vortex particles and/or the modification of the "vorticity charges" of the particles from the neighborhood. There is also a possibility to generate singular structures (in the form of small planar vortex sheets), which are replaced by "ordinary" particles if they move farther away from the boundary. Some of these ideas have been recently implemented and tested by Ploumhans *et al.* (2002).

7.   Summary and final remarks

The method of vortex particles proposed in this study has been tested on the standard example of a flow around a spherical body at moderate Reynolds numbers. In this part of the paper, we have focused on some technical and implementation details. The presented results are of preliminary character. Due to computing hardware limitations we were able to carry out calculations with a rather small number of the vortex particles. These circumstances affected the spatial resolution, but to a different extent in different flow regions. The dynamics of structures of the velocity in the wake area seems to be well reproduced. The large-scale motion remains in general agreement with the experimentally observed patterns of the flow. The major problem is the insufficient resolution of thin shear layers and the boundary layer at the body surface. It results in a serious underestimation of the surface-transversal velocity gradient and, consequently, friction forces. This problem appears because the vortex particles used in the numerical simulations were too large (in the sense of the spatial concentrations of their cores). Using much smaller particles would improve the spatial accuracy, but at the expense of currently intolerable increase of computational costs. Other methods of the enforcement of the no-

slip condition, based on some surface-fitted or even singular vortex element, can be incorporated in the future development of the proposed method.

References

1. BLELLOCH G., NARLIKAR G., 1997, A practical comparison of N-body algorithms – parallel algorithms, Series in *Discrete Mathematics and Theoretical Computer Science*, **30**

2. CHORLTON F., 1969,*Boundary Value Problems in Physics and Engineering*, Van Nostrand Reinhold Co., London

3. GARDINER C.W., 1990, *Handbook of Stochastic Methods*, 3rd Ed. Springer Verlag

4. GIBBON P., SUTMANN G., 2002, Long-range interactions in many-particle simulations, *Quantum Simulations of Complex Many-Body Systems*, **10**, 467-506

5. PLOUMHANS P., WINCKELMANS G.S., SALMON J.K., LEONARD A., WARREN M.S., 2002, Vortex methods for direct numerical simulations of three-dimensional bluff-body flows: application to the sphere at Re=300, 500, and 1000, *Journal of Computational Physics*, **178**, 427-463

6. PRINGLE G.J., 1994, Numerical study of three-dimensional flow using fast parallel particle algorithms, Ph.D. Dissertation, Departament of Mathematics, Napier University, Edinburgh

7. STYCZEK A., DUSZYŃSKI P., POĆWIERZ M., SZUMBARSKI J., 2004, Random vortex method for three dimensional flows. Part I: Mathematical background, *Journal of Theoretical and Applied Mechanics*, **42**, 1, 3-20

**Stochastyczna metoda wirowa dla przepływów trójwymiarowych.
Część II: Numeryczna implementacja i przykładowe wyniki**

Streszczenie

W drugiej częśći pracy omawiane są zagadnienia związane z implementacją metody wirowej w trzech wymiarach oraz prezentowane są wybrane wyniki obliczeń.

Testowym przykładem jest opływ kuli strumieniem jednorodnym. Opisano konstruk-
cję solwera zewnętrznego zagadnienia brzegowego typu Neumanna, proces generacji
nowych cząstek wirowych w pobliżu powierzchni ciała oraz sposób obliczania "stret-
chingu". Omówiono problem efektywnego obliczania prędkości indukowanej. Przed-
stawione wyniki, obejmujące chwilowe pola prędkości i wirowości oraz wybrane linie
prądu, demonstrują złożoność pola przepływu w śladzie za opływanym ciałem.